Phonon Localization by Mass Disorder in Dense Hydrogen-Deuterium Binary Alloy

Ross T. Howie,[1] Ioan B. Magdău,[1] Alexander F. Goncharov,[2] Graeme J. Ackland,[1] and Eugene Gregoryanz[1,*]
[1]School of Physics and Centre for Science at Extreme Conditions, University of Edinburgh, Edinburgh EH9 3JZ, United Kingdom
[2]Geophysical Laboratory, Carnegie Institution of Washington, 5251 Broad Branch Road NW, Washington, D.C. 20015, USA
(Received 23 June 2014; published 21 October 2014)

Using a combination of the Raman spectroscopy and density functional theory calculations on dense hydrogen-deuterium mixtures of various concentrations, we demonstrate that, at 300 K and above 200 GPa, they transform into phase IV, forming a disordered binary alloy with six highly localized intramolecular vibrational (vibrons) and four delocalized low-frequency (< 1200 cm^{-1}) modes. Hydrogen-deuterium mixtures are unique in showing a purely mass-induced localization effect in the quantum solid: chemical bonding is isotope-independent while the mass varies by a factor of 2.

DOI: 10.1103/PhysRevLett.113.175501 PACS numbers: 62.50.-p, 61.50.Ah, 61.50.Ks, 67.80.F-

Recently, a new phase of hydrogen (deuterium), phase IV, was discovered at 300 K and pressures above 230 GPa [1,2]. Phase IV has two characteristic vibrons in the Raman spectra [1,2]; by combining this observation with earlier density functional theory structure searches for phase III [3], it was proposed that this entropically stabilized phase consists of two alternating layers, graphenelike (G layer) and "freelike" diatomic molecules (B layer) [2,4–6] (see, also, [7]). The B layer in hydrogen has a characteristic high frequency vibron of $\nu_2 \sim 4100$ cm^{-1}, close to that in the gas state, and is a significant contributor to the zero-point energy (ZPE) compared with the much lower in energy ($\sim$2750 cm^{-1} at 310 GPa) ν_1 mode from the G layer. Deuterium mass lowers the ZPE by a factor of $\sqrt{2}$ ($\nu_2 \sim 3000$ cm^{-1} for D_2), posing some interesting physical questions about the behavior of dense hydrogen-deuterium mixtures in phase IV, since the two isotopes have quite different ZPE. It was theorized that ZPE gain from the vibrational modes could favor segregation of D_2 molecules to the B layer [3]. This segregation in 50:50 mixtures could lead to only two Raman-active vibrons with the B layer mode having the characteristic frequency of D_2, while the G-layer mode will have the characteristic frequency of H_2.

It is also possible that, in contrast to the ordering suggested by segregation, there could be atomic disorder with H_2, D_2 and hydrogen deuteride (HD) [which spontaneously forms at 300 K] distributed randomly across the lattice. In this case, the extreme isotopic mass ratio could raise another intriguing scenario: mass-induced Anderson localization of phonons. Anderson localisation [8–12] is an unusual phenomenon where sufficient disorder on the lattice can break the very concept of band structures. For phonons [12], this is due to either disordered bond strengths or disordered masses, or both. Scaling theory [13] shows that, in 3D, the eigenmode describing vibrations above a threshold frequency is not periodic and can become confined to a few atoms. This can be interpreted as strong scattering or interference of travelling waves, and in phonons, it has the effect of dramatically reducing thermal conduction. Because of the identical chemical bonding and huge mass ratio in hydrogen-deuterium mixtures, the possibility of localization exists, where the vibrational modes would be concentrated on a few molecules of a similar type.

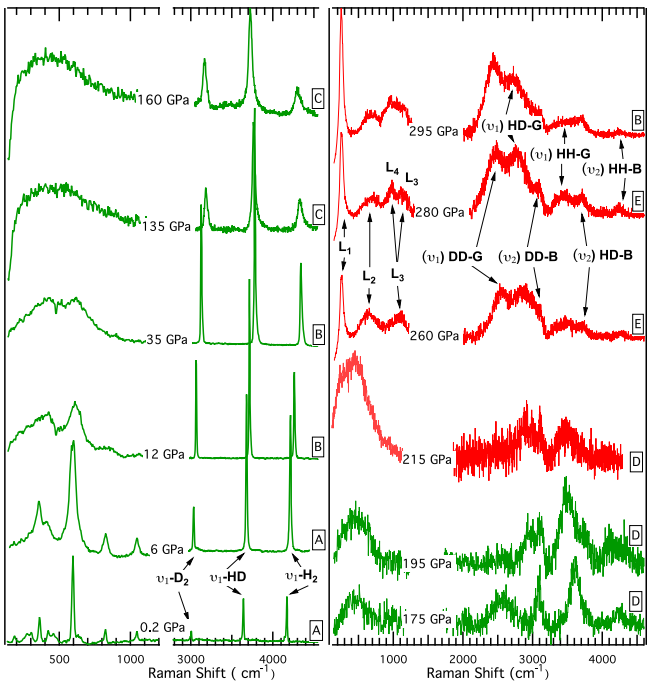

FIG. 1 (color online). Representative experimental Raman spectra of H_2-D_2 mixtures. The spectra from different runs at room temperature are labeled by the capital letters A, B, C, D, and E and marked with the nominal pressures at which spectra were collected. The strong first order diamond Raman at above 1333 cm^{-1} was removed for clarity. The spectra obtained with a 514 nm laser excitation line are shown in green while the spectra obtained with a 647 nm are shown in red. The ratio of the isotopes in run A is 60:40 (H:D); 55:45 in B and C, and 50:50 in D and E.

In order to investigate these possibilities, we have used Raman spectroscopy combined with density functional theory calculations on hydrogen-deuterium mixtures of varying concentrations (see Refs. [7,14–18] and references therein for the experimental and calculation details). At 300 K, for pressures as low as 0.2 GPa, Raman spectroscopy in the fluid shows three vibrational modes (ν_1) (Fig. 1), demonstrating the formation of HD molecules from an initial gas mixture of $H_2 + D_2$ (see, also, Ref. [19]). The low-frequency (< 1200 cm^{-1}) and vibrational modes of the mixtures correspond to a superposition of H_2, HD, and D_2 spectra up to ~195 GPa (Fig. 1). The low-frequency region at low pressures (< 20 GPa) shows a superposition of rotational excitations corresponding to three molecular types, while with an increase in pressure, the modes broaden and eventually smear out forming a single relatively weak and broad peak around 410 cm^{-1} (Fig. 1). In both experiment and calculations the Raman-active vibrons (ν_1-H_2, −HD, or D_2) are higher than in pure materials but below those of the infrared vibrations, approaching the latter ones in the limit of small partial concentration. [see Fig. 2(b) and Refs. [20–22]]. The ν_1-H_2, −HD, and D_2 depend on the composition (Figs. 2, 3 and Ref. [19]): the larger the molecular fraction—the closer the position of the vibrational band to that of a pure material, while the bands corresponding to smaller partial composition (impurity) have a higher frequency. This observation can be partially understood based on the vibrational coupling model [23,24], according to which the vibrational frequency is lowered due to the intermolecular coupling.

Above ~195 GPa, the Raman spectrum starts to change drastically and cannot be described as a superposition of H_2, D_2, and HD spectra. Between 195 and ~210 GPa, the broad peak at ~410 cm^{-1} and vibrational (ν_1) modes split (Figs. 1 and 2), suggesting a phase transformation to phase IV. The splitting is similar to that observed in pure H_2 or D_2 [2], although the splitting in mixtures appears to happen at slightly lower pressures. At pressures above 220 GPa, the low-frequency region forms three well-defined relatively narrow bands [marked $L_{1,2,3}$ in Figs. 1 and 2(a)] with $L_1 \sim 250$ cm^{-1} becoming sharper and more intense with increasing pressure. At 270 GPa, the $L_3 \sim 1100$ cm^{-1} mode splits off to form L_4 [Figs. 1, 2(a)] indicating the appearance of phase IV′, as documented for the pure H_2 [25]. If the

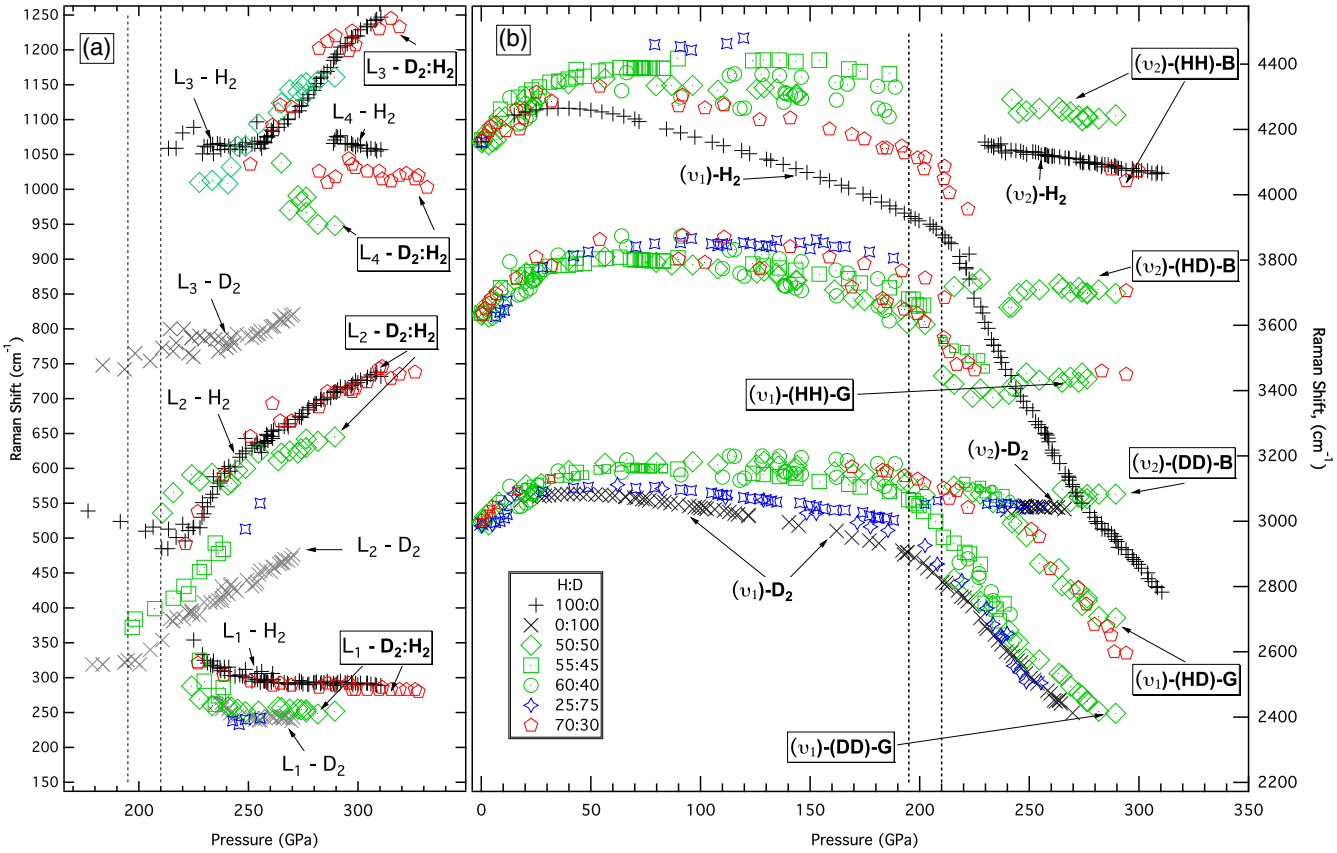

FIG. 2 (color online). Experimental pressure dependencies of the Raman low-frequency (a) and vibrational (b) bands observed in H_2-D_2 mixtures. The colored symbols represent the frequencies from the mixtures and the grey "crosses" and black "plus" mark the frequencies of pure D_2 and H_2 from Refs. [2,25]. The same color represents the same ratio of H:D with the exact numbers given in the legend. The vertical black dashed lines at 195 and 210 GPa indicate the pressure range at which low frequency and vibrational modes undergo significant changes and split.

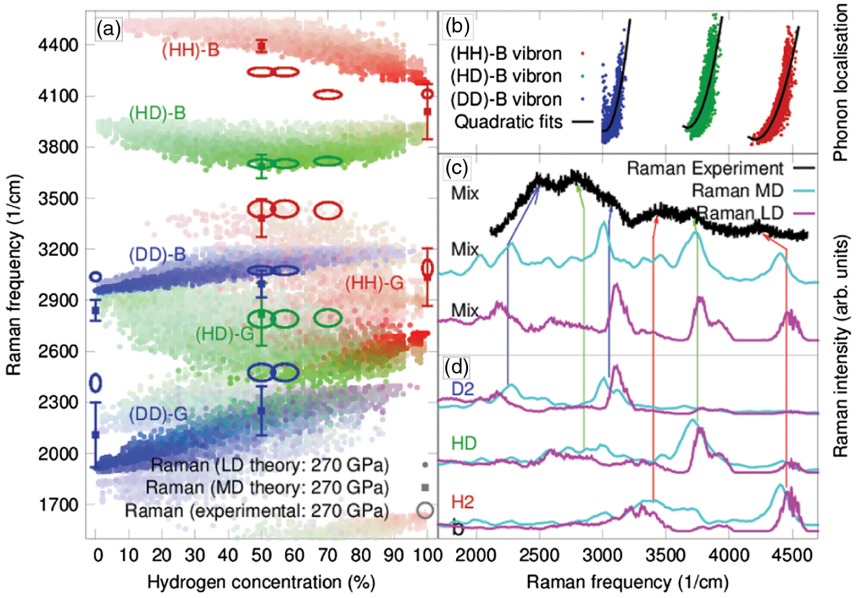

FIG. 3 (color online). Comparison of calculated and measured Raman spectra at 270 GPa. (a) The most intense Raman modes for 2700 different LD calculations (one colored solid dot per mode) at 270 GPa and various concentrations. The color is assigned by calculating red/green/blue ratios based on the partial Raman contributions from each molecular species: H_2 (red), HD (green), and D_2 (blue) with the saturation proportional to the Raman intensity. The Raman experimental data is plotted with ellipses where the axes represent the errors in concentration and frequency. Colors demonstrating the character of each mode were attributed by observing the behavior of the spectra with pressure in the experiments. MD (colored solid rectangles) show peaks of the Fourier-transformed autocorrelation projection function. Differences from the LD come from including dynamical effects such as the librations of trimer motifs (see, also, [7]). (b) The dependency of the B vibron frequency on total phonon localization for H_2, HD, and D_2, at various concentrations and 270 GPa. A clear pattern emerges: the higher the frequency of the mode, the larger its localization becomes (see, also, Fig. S3). (c) Detailed theory-experiment comparison of the Raman spectra at 270 GPa and 50:50% H_2-D_2 mixtures. Experimental resolution error is not included in the MD and LD results. (d) Individual contributions of different molecular species calculated with both LD and MD. The correspondence between individual modes is illustrated with arrows.

H_2/D_2/HD isotopes were phase separated, 12 low-frequency and six vibrational modes would have been observed instead. If the H_2/D_2 were segregated, then only two vibrational modes would have been present, but there is no evidence for either. We note that with precisely four distinct modes, the low-frequency region for mixtures is equivalent to that of a single pure isotope in phase IV [2], indicating that all atomic species participate in these modes. The observed vibrational part of the spectrum can only be explained by contributions from H_2, D_2, and HD molecules in both *G* and *B* layers [Figs. 2(b), 3]. Following this scheme, the isolated *B*-layer peaks can be identified by simple mass scaling and by their slightly narrower appearance (Fig. 1). However, the assignment of the *G*-layer peaks is not straightforward since the observed lower-frequency vibrational modes form a complex density of statelike patterns (Figs. 1, 2, and 3), and their widths increase with pressure causing modes to overlap (Fig. 1). But more interestingly, the pressure dependence of the (ν_1) HD-*G* mode frequencies appears as a natural continuation of the (ν_2) DD-*B* mode, while (ν_1) HH-*G* appears as the continuation of (ν_2) HD-*B* vibration [Fig. 2(b)] (HH and DD refer to modes primarily involving stretches of HH (DD) bonds. i.e., H = hydrogen, D = deuterium, HH = hydrogen − hydrogen). Being the lightest, H_2 scatters and couples the most, and the HH-*G* mode is extremely broad and surprisingly pressure independent, its mean value persisting at frequencies around 3450 cm^{-1}. The HH-*G* band also appears to be relatively weaker and broader (due to redistribution of its intensity) than the ones from D_2 and HD.

We analyzed the disordered system using *ab initio* lattice dynamics (LD) (at $T = 0$ K) and molecular dynamics (MD) ($T = 300$ K) simulations of phase IV, based on the P_c structure [4]. Free energy calculations from LD (Fig. S1 [7]) show that the ZPE gain in the vibron modes is offset by frequency shifts elsewhere, and the free energy of ordering is too small to drive isotopic segregation, consistent with experimental observation of six peaks. Our LD calculations demonstrate that the mass disorder gives vibron eigenmodes very different frequencies from the pure isotopes, exhibiting a strong localization tendency. The precise amount of localization decreases as the isotope concentration (see Figs. 4 and S2 in [7]) increases. The contribution of different species within a single mode varies: the HH-*B* and HD-*B* modes typically involve only

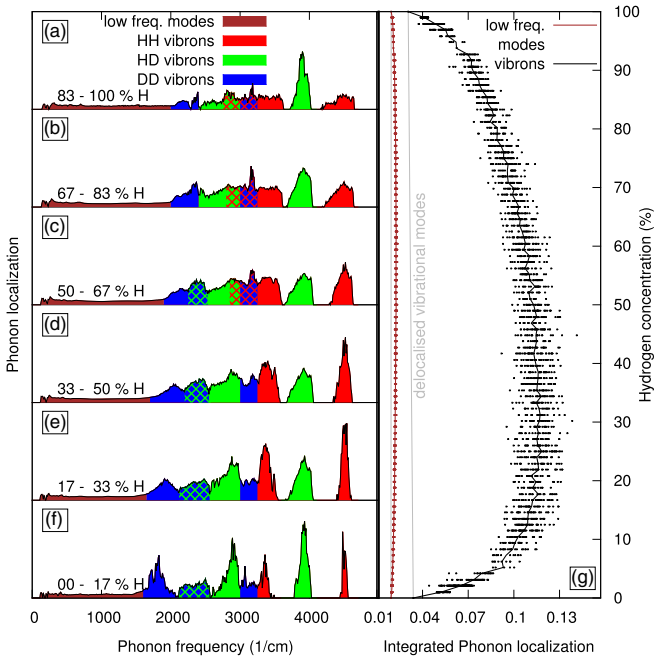

FIG. 4 (color online). Calculated phonon localization at 270 GPa. Panels (a)–(f): Calculated localization inverse participation ratio per mode as a function of frequency for different H concentration ranges. Shaded brown areas are the low-frequency modes, that show no localization. Red, green, and blue shades indicate vibrons involving mainly H_2, HD, and D_2, respectively, with considerable overlap for D_2-B and G modes. Panel (g): Localization as a function of concentration for vibrational (black) and low-frequency modes (brown). Inverse participation ratio (Ref. [7]) from the delocalized limit of pure H_2 and D_2, are illustrated in light grey. The skewed maximum shows that isolated H_2 molecules in the B layer produce strongly localized vibrations, whereas isolated B-layer D_2 molecules couple to HD and H_2 molecules in the G layers (H_2 molecules are more likely to be isolated if their concentration is low).

one species, whereas the *G*-layer vibrons involve all molecular types, except for high D concentrations where the DD-*G* mode is at a distinct (Fig. 3) frequency.

We see in Fig. 4 that the localization leads to broadening of the phonon bands: HH (DD) modes have the widest range of values at high H (D) concentration, while HD modes are broadest around 50-50 mixtures, where the HD molecule is the most common species. We also carried out a detailed theoretical analysis of vibrational eigenvectors to determine the Raman activity of modes using the projection method [6,17]. This shows that localization causes many more modes to acquire Raman activity than is the case for H_2 and D_2. This is in excellent agreement with our Raman spectra which show broad vibrons in the *G* layers and narrow uncoupled *B* bands (Fig. 1), all of which are much broader than in HH or DD.

Within a band of modes, the Raman activity is still in the in-phase modes which are typically lower frequencies. Thus, the effect of broadening the entire band is to lower the frequencies of the Raman active modes. So increased localization lowers the frequencies of the Raman active modes. Since localization varies with concentration, this gives a measurable variation in the Raman shift with concentration. In Fig. 3, we compare these predictions with experimental results at similar conditions: *ab initio* LD predictions are in excellent agreement with experiments for the peak widths, and the variation in Raman shifts with concentration and pressure. The Raman frequencies for the *B*-layer vibrons are also in good agreement. The *G*-layer frequencies are too low, but as previously reported [6], MD calculations introduce the anharmonic coupling needed to improve the agreement.

Two well separated, nearly pressure-independent, bands near 4300 and 3700 cm^{-1}, come from HH-*B* and HD-*B* vibrations, respectively. The HH-*B* vibrational mode frequencies are predicted and observed to decrease with increased H concentration as the modes become less localized, while the HD-*B* modes have a minimum frequency at 50% (Fig. 3). By inspecting the eigenvectors (Fig. S3 [7]), we conclude that the H_2 molecules in the *B* layer vibrate in separate groups of 2–3 molecules at frequencies weakly dependent on the neighboring environment. As the H concentration increases, the different H_2 islands grow and start coupling, reducing the Raman frequency. For similar reasons, the HD-*B* mode is softest around 50:50 mixtures when HD molecules are most abundant. The DD-*B* vibration couples to the HH-*G* vibration in LD calculation. However, in MD, the *G*-layer vibrations have higher frequencies, and thus, DD-*B* is coupled more strongly to HD-*G* modes (Fig. 3). This explains why HD-*G* overlaps with the DD-*B* mode in the experiment [Fig. 2(b)]. By contrast, the *G* modes are more delocalized and strongly hybridized. Above 50% H concentration, DD-*B*, HH-*G*, and HD-*G* have very similar frequencies and generate a broad, complex Raman-signal as seen experimentally. Eigenmodes can no longer be assigned to a single molecular species, in particular, the HH-*G* mode couples heavily to the HD-*G* vibrations. Because of this strong coupling, HH-*G* does not show the characteristic softening with increasing pressure [Figs. 2(b), and S4, S5 in [7]].

As shown previously [6], the Raman frequency of the *G* vibrations is sensitive to temperature. We used MD projection to investigate this ([7]); we see that temperature increases the frequency shifts into better agreement with experiment. The MD shows localization, but does not permit the necessary level of configurational sampling for quantitative analysis of concentration and distribution. We do not see any mode localization for the low-frequency ($L_{1,2,3,4}$) excitations [Figs. 2(a) and 4]. These modes either involve motion of large units such as *G*-layer trimers or interlayer modes. The L_1 mode (trimer-libration) characteristic of phase IV in pure $H_2(D_2)$ is observed following either the pure H_2 frequencies in the H rich mixtures or D_2

frequencies in 50:50 and D rich samples [Fig. 2(a)]. This observation is in agreement with the highly anharmonic nature of these modes [6,25,26].

The agreement of frequencies and widths is evidence that simulation and experiment are looking at the same phase IV structure. The key observable signature of localization lies in the concentration dependence (Figs. 2 and 3). For each species (H_2, HD, and D_2) more-localized modes have a higher Raman frequency; thus, the H_2 data [Fig. 3(a)] have a negative slope, the D_2 data positive, and the HD peaked at about 50% concentration.

Anderson localization has been demonstrated in several systems including light [27], sound [28], and Bose-Einstein condensates [29]. This Letter has turned the spotlight onto the equivalent phonon phenomenon, driven purely by mass disorder. Hydrogen isotopes are the only physical candidate for Anderson localization of phonons due only to isotope mass. Indeed, for simple lattices, even a 2:1 mass ratio is insufficient to cause localization [12]; however, the inhomogeneity between inter-and intramolecular bonds circumvents this theoretical limit allowing localization of vibrons in $H_2/HD/D_2$ mixtures. Phase IV of hydrogen(s) is a unique system where there is a crossover between intramolecular, intermolecular, and quantum energy scales with the ratio of phonon energies almost 20:1, providing the route for the localization despite the mass ratio of 2:1.

This work was supported by a research grant from the U.K. Engineering and Physical Sciences Research Council. A. F. G. acknowledges support from the NSF.

*e.gregoryanz@ed.ac.uk

[1] M. I. Eremets and I. A. Troyan, Nat. Mater. **10**, 927 (2011).
[2] R. T. Howie, C. L. Guillaume, T. Scheler, A. F. Goncharov, and E. Gregoryanz, Phys. Rev. Lett. **108**, 125501 (2012).
[3] C. J. Pickard and R. J. Needs, Nat. Phys. **3**, 473 (2007).
[4] C. J. Pickard, M. Martinez-Canales, and R. J. Needs, Phys. Rev. B **85**, 214114 (2012).
[5] H. Liu, L. Zhu, W. Cui, and Y. Ma, J. Chem. Phys. **137**, 074501 (2012).
[6] I. B. Magdau and G. J. Ackland, Phys. Rev. B **87**, 174110 (2013).
[7] See Supplemental Material at http://link.aps.org/supplemental/10.1103/PhysRevLett.113.175501 for the experimental, molecular and lattice dynamics calculations details.
[8] F. J. Dyson, Phys. Rev. **92**, 1331 (1953).
[9] P. W. Anderson, Phys. Rev. **109**, 1492 (1958).
[10] A. Lagendijk, B. van Tiggelen, and D. Wiersma, Phys. Today **62**, 24 (2009).
[11] F. Evers and A. D. Mirlin, Rev. Mod. Phys. **80**, 1355 (2008).
[12] C. Monthus and T. Garel, Phys. Rev. B **81**, 224208 (2010).
[13] E. Abrahams, P. W. Anderson, D. C. Licciardello, and T. V. Ramakrishnan, Phys. Rev. Lett. **42**, 673 (1979).
[14] Y. Akahama and H. Kawamura, J. Phys. Conf. Ser. **215**, 012195 (2010).
[15] M. Marqués, M. Santoro, C. L. Guillaume, F. A. Gorelli, J. Contreras-García, R. T. Howie, A. F. Goncharov, and E. Gregoryanz, Phys. Rev. B **83**, 184106 (2011).
[16] F. A. Gorelli, S. F. Elatresh, C. L. Guillaume, M. Marqués, G. J. Ackland, M. Santoro, S. A. Bonev, and E. Gregoryanz, Phys. Rev. Lett. **108**, 055501 (2012).
[17] G. J. Ackland and I. B. Magdau, High Press. Res. **34**, 198 (2014).
[18] R. T. Howie, E. Gregroyanz, and A. F. Goncharov, J. Appl. Phys. **114**, 073505 (2013).
[19] D. M. Brown and W. B. Daniels, Phys. Rev. A **45**, 6429 (1992).
[20] P. Loubeyre, F. Occelli, and P. Dumas, Phys. Rev. B **87**, 134101 (2013).
[21] M. I. Eremets, I. A Troyan, Ph. Lerch, and A. Drozdov, High Press Res. **33**, 377 (2013).
[22] C. S. Zha, Z. Liu, M. Ahart, R. Boehler, and R. J. Hemley, Phys. Rev. Lett. **110**, 217402 (2013).
[23] J. van Kranendonk, *Solid Hydrogen. Theory of the Properties of Solid H_2, HD and D_2* (Plenum Press, New York, 1983).
[24] P. Loubeyre, R. LeToullec, and J. P. Pinceaux, Phys. Rev. B **45**, 12844 (1992).
[25] R. T. Howie, T. Scheler, C. L. Guillaume, and E. Gregoryanz, Phys. Rev. B **86**, 214104 (2012).
[26] A. F. Goncharov, J. S. Tse, H. Wang, J. Yang, V. V. Struzhkin, R. T. Howie, and E. Gregoryanz, Phys. Rev. B **87**, 024101 (2013).
[27] M. Segev, Y. Silberberg, and D. N. Christodoulides, Nat. Photonics **7**, 197 (2013).
[28] H. Hu, A. Strybulevych, J. H. Page, S. E. Skipetrov, and B. A. van Tiggelen, Nat. Phys. **4**, 945 (2008).
[29] G. Roati, C. D'Errico, L. Fallani, M. Fattori, C. Fort, M. Zaccanti, G. Modugno, M. Modugno, and M. Inguscio, Nature (London) **453**, 895 (2008).